ACS APPLIED MATERIALS & INTERFACES

Research Article

www.acsami.org

Influence of Cu Vacancy on Knit Coir Mat Structured CuS as Counter Electrode for Quantum Dot Sensitized Solar Cells

A. Dennyson Savariraj,[†] Kodakkal Kannan Viswanathan,[‡] and Kandasamy Prabakar*,[†]

[†]School of Electrical Engineering, Pusan National University, San 30, Jangjeong-Dong, Gumjeong-Ku, Busan 609 735, South Korea

[‡]UTM Centre for Industrial and Applied Mathematics, Deparment of Mathematical Sciences, Universiti Teknologi Malaysia, 81310 Johor Bahru, Johor, Malaysia

ABSTRACT: Knit-coir-mat-like structured CuS thin films prepared by chemical bath deposition with different time duration were used as counter electrode in qunatum dot sensitized solar cells. The film deposited at 4 h exhibited better electrochemical and photovoltaic performance with J_{SC}, V_{OC}, and FF values of 14.584 mA cm^{-2}, 0.566 V, and 54.57% and efficiency of 4.53%. From the UV−vis absorption spectra, it is observed that CuS thin film exhibits free carrier intraband absorption in the longer wavelengh region. The enhanced performance of CuS counter electrodes is due to Cu vacancies with increased S composition, and the quasi-Fermi energy level in semiconductors with respect to electrolyte redox potential is one of the causes that affects the electrocatalytic activity of counter electrodes.

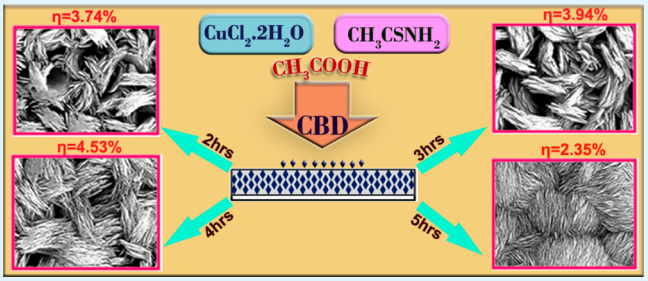

KEYWORDS: *CuS counter electrodes, quantum dot solar cells, impedance spectroscopy, knit coir mat*

1. INTRODUCTION

The rapid increase in the global population and the corresponding energy need to be addressed productively using nonrenewable energy sources. The exorbitant production cost of thin film solar cells irrespective of high power conversion efficiency resulted in finding dye sensitized solar cells (DSSC) as a low-cost alternative by O'Regan and Gratzel in 1991.[1−3] The photodegradation and instability of DSSC paved the way for the search of third generation photon harvesters, namely quantum dots (QDs), with enhanced efficiency and device stability having advantages over DSSC.[4] QDs are semiconducting materials having advantages of size dependent tunable band gap with quantum confinement to suit the spectrum of sunlight,[5] with multiple excitation generation due to impact ionization[6,7] and hot-carrier transfer,[8] higher extinction coefficients, and larger intrinsic dipole moments[4] leading to charge separation, which all make them superior over organometallic dyes.[3] Even with the above-mentioned advantages, the photovoltaic performance of quantum dots sensitized solar cells (QDSSC) is still behind that of DSSCs accounting for the electron loss occurring due to charge recombination at the TiO_2/electrolyte and photosensitizer (QD)/electrolyte interfaces.[8,9] Similar to DSSC, QDSSC makes use of a range of wide band gap materials such as TiO_2,[1] ZnO,[10] SnO_2,[11] and Nb_2O_5[12] as photoanodes. The iodide/tri-iodide (I^-/I^{3-}) electrolyte used in DSSC is not a suitable candidate for QDSSC as it causes photocorrosion to the QDs,[13] and therefore, polysulfide (S^{2-}/S_n^{2-}) is more preferred for QDSSC over I^-/I^{3-} to minimize photocorrosion.[14−16] Moreover, platinum (Pt) proves to be a successful candidate as a CE for DSSC with appreciable electrocatalytic activity for the redox of iodine/triiodide, exhibiting minimum resistance;[17] however, it has very low electrocatalytic activity toward polysufide electrolyte[18−20] making it handicapped as CE for QDSSC irrespective of the method of preparation. Although Pt has very high conductivity, physical adsorption of sulfur-containing group onto the surface of Pt causes catalytic poisoning resulting in poor electrocatalytic activity, and leading to high over potential which hinders the reduction of the oxidized redox species of the electrolyte and rapidly reduces the cell's performance.[18,21] This leaves the researchers to find a cost-effective alternative to Pt with maximum electrocatalytic activity and low charge transfer resistance (R_{CE}). Until now, there have been several alternatives to Pt reported as CE, to achieve high charge separation and electrocatalytic activity. Counter electrodes play a major role in collecting the electron from the external circuit and reducing the S_n^{2-} ions to S^{2-}.[18,22−28] To eliminate the previously mentioned drawback, carbon nanotubes,[29] graphene,[30] mesocellular carbon foam,[31] and p-type metal chalcogenide materials PbS,[27,32] CoS,[26,33] NiS,[33] and CuS[18,26,33−35] are used to facilitate hole capture at the counter electrode and to boost up the efficiency of QDSSC since they have a large area deposition capability. While there are many alternatives, CuS is most preferred since it not only yields high efficiency[23] but also is cost-effective and has superior photo- and electrocatalytic property and conductivity as well.[26,36,37]

Received: July 17, 2014
Accepted: October 24, 2014
Published: October 24, 2014

Cu_2S is an unstable phase due to the formation of Cu vacancies even in thermodymanic equilibrium with bulk copper metal.[38] Even though CuS is a p-type semiconductor, it exhibits mixed electronic and ionic conduction due to the presence of Cu vacancies that give rise to free holes which act as electron acceptors exhibiting high conductivity.[39,40] Moreover, CuS composition varies from S-rich (CuS_2) to Cu-rich (Cu_2S) exhibiting different morphologies.[41−43] We found that surface morphology and Cu:S ratio are affected with deposition time. In polysulfide, the CE interface plays a major role in enhancing the electrocatalytic activity. Hence, it is highly essential to understand whether surface morphology and/or Cu:S ratio affect the electrocatalytic activity of CuS films used in QDSSC as CE. To the best of our knowledge, composition and surface morphology dependent electrocatalytic activity applied to QDSSC have not been reported and hence are our work. Herein, we report time varied chemical bath deposited knit coir mat structured CuS thin films as CE for QDSSCs photovoltaic performance which are found to surpass our previous work with Pt/CuS[44] and CuS/CoS CE[26] having an efficiency (η) of 4.53%.

2. EXPERIMENTAL SECTION

Densely packed knit-coir-mat-like structured CuS thin films were deposited on well-cleaned fluorine doped tin oxide (FTO) glass substrates with a sheet resistance of 7 Ω/cm^2 (Hartford Glass) by chemical bath depositon (CBD) using aqueous solutions of copper chloride dihydrate ($CuCl_2 \cdot 2H_2O$) and thioacetamide (CH_3CSNH_2) as copper and sulfur sources, respectively. All the precursors used for the synthesis were analytical grade and purchased from Sigma-Aldrich, and the synthesis was carried out without further purification. In 25 mL of deionized water (DI), 0.10 M of copper chloride dihydrate ($CuCl_2 \cdot 2H_2O$) was dissolved (solution A) and 1.0 M of thioacetamide (CH_3CSNH_2) were dissolved in 25 mL of deionized water (solution B) separately and vigorously stirred for 30 min to get a transparent solution. The two transparent solutions were mixed with constant stirring, and to this solution was added 0.85 M acetic acid (CH_3COOH) in drops; the reaction mixture was stirred vigorously for 1 h. The previously cleaned FTO glass substrates were immersed in to the growth solution horizantally and placed in a hot air oven. The deposition was carried out at a constant temperature of 60 °C for a period of 2, 3, 4, and 5 h, and the deposited CuS films were labeled as CE2, CE3, CE4, and CE5, respectively.

2.1. Fabrication of TiO_2/CdS/CdSe/ZnS Photoanode. The FTO substrates were cleaned ultrasonically and used for the fabrication of photoanode. Porous TiO_2 films were coated on FTO from commercially available TiO_2 paste of particle size 20 nm (Ti-Nanoxide HT/S, Solaronix) by doctor blade method with an active area of 0.27 cm^2, after which it was annealed at 450 °C for 30 min. The TiO_2 coated photoanodes were cosensitized with CdS and CdSe QDs using successive ionic layer adsorption and reaction (SILAR). Solutions of 0.025 M cadmium acetate dehydrate ($Cd(CH_3COO)_2 \cdot 2H_2O$) and 0.2 M sodium sulfide (Na_2S) were prepared for the Cd^{2+} and S^{2-} ion sources, respectively, for CdS QD. The TiO_2 coated photoanode was immersed in to cadmium acetate dihydrate solution for 5 min, in order to adsorb Cd^{2+} ions onto the TiO_2 surface, rinsed with DI water and ethanol to remove the excessively adsorbed cations, and dried under N_2 gas. The Cd^{2+} adsorbed photoanodes were then immersed in the Na_2S solution for 5 min, to adsorb S^{2-} ions on to the photoanode and to react with previously adsorbed Cd^{2+} ions to form CdS QD, followed by rinsing with DI water and ethanol to remove the excess anions, and dried with N_2 gas. This completes 1 cycle, and 5 such cycles were done to deposit CdS QDs on the photoanode. Then, 8 cycles of CdSe QDs were deposited using the above-mentioned SILAR method, with 0.025 M of cadmium sulfide ($Cd(CH_3COO)_2 \cdot 2H_2O$ and 0.2 M selenium (Se) for cation and anion sources, respectively. The QD-sensitized photoanodes were finally dipped in 0.2 M of zinc nitrate hexahydrate ($ZnNO_3 \cdot 6H_2O$) and 0.2 M of Na_2S alternatively and dried with N_2 gas to deposit a zinc sulfide (ZnS) passivation layer to avoid corrosion of QDs due to the electrolyte and to prevent back electron transfer into the electrolyte.

2.2. Fabrication of QDSSCs and Symmetric Cells. The CdS/CdSe/ZnS photoanodes and a counter electrode (CuS and Pt) were sandwiched between a 25 μm hot-melt sealing sheet (SX 1170-25, Solaronix). By capillary action, the internal space was filled with a redox liquid electrolyte of 1 M of Na_2S, 2 M of S, and 0.2 M of KCl in a mixture of 3 mL of deionized water and 7 mL of methanol.

The symmetric electrodes of CuS and Pt films were sandwiched between a 25 μm hot-melt sealing sheet (SX 1170-25, Solaronix) and filled with a redox liquid electrolyte 1 M of Na_2S, 2 M of S, and 0.2 M of KCl in a mixture of 3 mL of DI water and 7 mL of methanol.

3. CHARACTERIZATION TECHNIQUES

The structure and phase purity of the synthesized CuS films were analyzed by X-ray diffraction (XRD; Bruker D8-Advance) with Cu Kα radiation (λ = 1.540 56) source operated at 40 kV and 30 mA in the range 20−80°. The surface morphology of the sample was analyzed using FE-SEM (Hitachi, model S-4200) operated at 15 kV. X-ray photon spectroscopy (XPS) was performed using a VG scientific ESCALAB250 with monochromatic Al Kα radiation of 1486.6 eV and with an electron take off angle of 90°. The pressure of the chamber was kept at 10 $^{-10}$ Torr during the measurement. The survey spectrum was scanned in the binding energy (BE) range 0.0−1400 eV in steps of 1 eV. The binding energy values reported here are relative to the carbon C 1s core level at 284.6 eV. UV−vis spectroscopic analysis was carried out using an Optizen 3220 UV spectrophotometer. The current−voltage charecteristics of the QDSCs were studied under 1 sun illumination (AM 1.5G 100 mW cm^{-2}) using ABET Technologies solar stimulator having the irradiance uniformity of ±3%. Cyclic voltammetry and electrochemical impedance spectroscopy (EIS) were performed using a BioLogic potentiostat/galvanostat/EIS analyzer (SP-150, France) under 1 sun illumination.

4. RESULTS AND DISCUSSION

Figure 1 features the X-ray diffraction pattern of CuS thin films on the FTO substrate. Some of the peaks of the CuS thin films were overlapping with the peaks arising from the FTO. The diffracted peaks of (105), (008), (110), (206), and (212) are corresponding to hexagonal CuS and match well with ICDD file no. 79-2321.[43] The compound is confirmed to be covelite

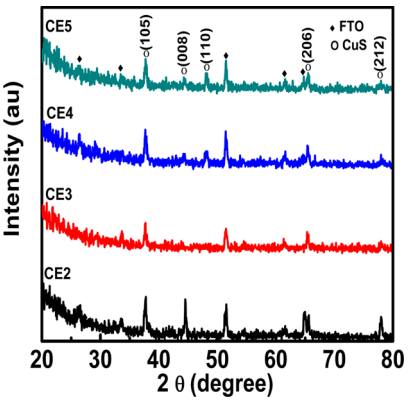

Figure 1. X-ray diffraction spectrum of CuS thin films deposited on FTO substrates.

Figure 2. SEM images of CuS thin films deposited on FTO substrates.

Table 1. Cu:S Composition, EIS of Symmetrical Dummy Cells, and QDSSC and IV parameters

		EIS for symmetric cell						EIS parameters for QDSSCs			
cell	composition Cu:S (at. %)	R_s (Ω)	R_{CE} (Ω)	*Voc* (V)	*Jsc* (mA/cm^2)	FF (%)	η (%)	R_s (Ω)	R_{CE} (Ω)	R_{CT} (Ω)	τs (ms)
CE2	51.27:48.73	5.16	25.22	0.552	11.857	56.84	3.74	7.71	3.98	28.4	31.05
CE3	49.28:50.72	6.0	27.25	0.574	12.376	55.18	3.94	8.08	5.81	31.24	34.80
CE4	41.27:58.73	4.13	1.04	0.566	14.584	54.57	4.53	6.99	1.84	17.35	41.94
CE5	56.4:43.6	7.28	48.75	0.561	08.692	46.98	2.35	9.67	8.34	43.2	21.12
Pt		8.83	576.23	0.559	06.671	31.71	1.45	9.86	12.32	418.47	0.33

CuS because the key peaks at 46.1° and 48.6° correspond to both $Cu_{1.97}S$ and $Cu_{1.8}S$, and the peak at 37° which is exclusively present in $Cu_{1.97}S$ is absent.[43] For CE2, the peak at 44.4° corresponding to the (008) plane has the highest intensity, whose intensity gets reduced, and the full width at half-maximum increased upon increasing the deposition time from 3 to 5 h. This suggests that CE2 is more crystalline which is reduced when we go from CE2 to CE5 owing to the increase in the film thickness. Moreover, the peak at (110) is absent for CE2 and CE3 whereas it is present in CE4 and CE5. This might have been caused by phase change during the growth of the samples over 3 h as it is well-evidenced from the SEM pictures. The reaction involves homogeneous nucleation followed by heterogeneous film deposition on to the FTO substrate. There has been no deposition of the film until 1 h; deposition began after 1 h, and the film gets peeled off after 5 h. The reaction follows the following mechanism.

$$CuCl_2 \rightarrow Cu^{2+} + 2Cl^- \quad (1)$$

Thioacetamide reacts with H_2O and dissociates to give H_2S.

$$CH_3{-}CS{-}NH_2 + H_2O \rightarrow CH_3{-}CO{-}NH_2 + H_2S \quad (2)$$

$$H_2S + H_2O \rightarrow SH^- + H_3O^+ \quad (3)$$

$$SH^- + H_2O \rightarrow S^{2-} + H_3O^+ \quad (4)$$

$$Cu^{2+} + S^{2-} \rightleftarrows CuS \quad (5)$$

Figure 2 shows the scanning electron microscopy (SEM) images of the CuS thin films deposited on the FTO substrates by chemical bath deposition for period of 2−5 h. It reveals that the surface morphology is greatly influenced by the deposition time. As seen, when the deposition time was 2 h (CE2), a bunch of nanoplatelets with tubelike sturcture are formed. As the deposition time increases, the space between the nanoplatelets was reduced with increased interpenetrated knit-coir-

mat-like structure at 5 h (CE5) deposition time. It is peculiar in structure with a progressive structural change from an array of nanoplatelets to knit-coir-mat-like structure. The films CE2 and CE3 have less densely packed assembly of nanoplatelets with huge voids. The increase in the deposition time to 4 h (CE4) makes them denser, and the voids in between the nanoplatelets have been reduced with uniform pores and with 5 h (CE5) of deposition; the film grows like a well-knit-coir-mat-like structure without any pore. Table 1 shows the composition of the as-deposited films, indicating an increase in S with increased deposition time until 4 h, after which Cu^{2+} ion concentration dominates, and this reduces S as is seen in CE5.

The absorption spectra of the CuS thin films (Figure 3a) show that CE2 and CE3 have an absorption minimum at 646,

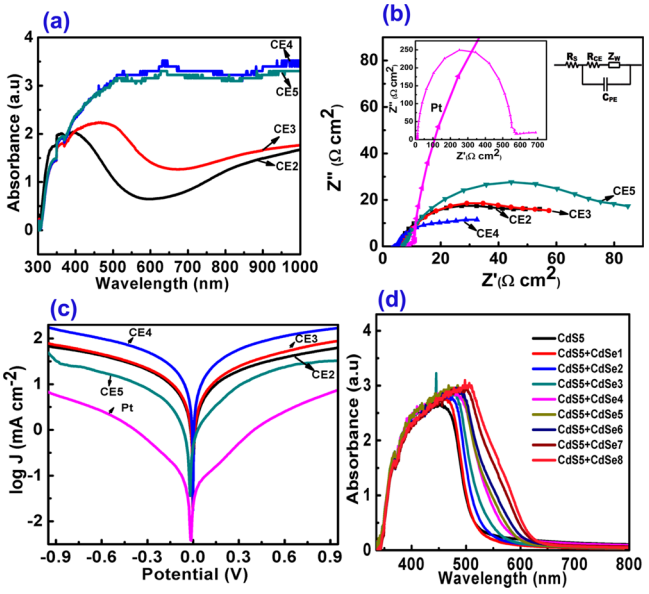

Figure 3. (a) UV absorption spectra of CuS thin films deposited on FTO substrates coated by CBD. (b) Nyquist plot for CuS and Pt electrode symmetrical cells: inset shows magnified plot of Pt and equivalent circuit. (c) Tafel polarization plot for CuS and Pt electrodes symmetrical cells. (d) UV absorption spectra of TiO_2/CdS/CdSe/ZnS cascade photoanode deposited by SILAR method.

816 nm, respectively, while CE4 and CE5 absorb strongly due to high thickness and lie beyond instrument limitation. The increased absorption at longer wavelength region is due to free carrier intraband absorption.[43,45]

EIS measurements were carried out for the symmetrical dummy cell composed of two identical CuS CEs with polysulfide electrolyte as shown in Figure 3b with equivalent circuit. In the circuit, R_s is the series resistance, R_{CE} is the charge transfer resistance at CE/electrolyte interface, C_{PE} is the corresponding capacitance, and Z_W is the Warburg impedance of the redox electrolyte.[23,26,29] The measurements were carried out at open circuit bias potential in the frequency range 100 mHz−500 kHz. The impedance data were fitted using the equivalent circuit shown in the inset, and extracted parameters are given in Table 1. The R_{CE} is responsible for charge exchange between the CE and polysulfide electrolyte. Pt has the highest R_{CE} value of 576.23 Ω while all the other CuS CEs have much smaller R_{CE} values, showing the superior electrocatalytic activity of CuS over Pt.[43]

Among the CuS CEs, a decrease in the R_{CE} value was observed until CE4 which exhibits the lowest R_{CE} of 1.042 Ω and ensures higher electrocatalytic activity of CE4. R_s is a measure of the electronic adhesion of the CE onto FTO and is inclusive of its sheet resistance. Pt has an R_s value of 8.83 Ω while CE4 has the lowest value of 4.13 Ω, suggesting very low contact resistance and possibly conducting the charge carriers with very low loss. The diffusion impedance (Z_W) is also a measure of electrocatalytic activity as it is inversely proportional to the reduction of polysulfide electrolyte. The Z_W values of CE2, CE3, CE4, CE5, and Pt CEs are 8.15, 10.48, 3.65, 20.58, and 102.58 Ω, respectively. CE4 has the lowest Z_W value of 3.65 Ω that suggests it has a very high rate of reducing the polysulfide electrolyte; on the contrary, Pt CE (102.80 Ω) is found to poorly catalyze the reduction of polysulfide. The reason for the poor reduction of polysulfide by Pt is due to the physisorption of S ions onto the Pt surface leading to catalytic poisoning. This hinders the cell's performance and affects the cell's efficiency.

Figure 3c shows the Tafel measurement of the symmetrical cells made of CuS CEs and Pt CE. It is a measurement of logarithmic current density as a function of applied potential. The Tafel plot consists of three zones: the first one is the polarization zone at the lower potential (−Ve), the second is the Tafel zone at the middle with a steep slope, which is the fingerprint of catalytic ability of the CE, and the third one is due to diffusion region at the higher voltage. The extrapolation of the linear region of the curve to zero gives the exchange current density (J_0). The limiting current density (J_{lim}) can be derived from the curve at high potential region. From these parameters, the electrochemical catalytic behavior of the CEs can be inferred. The current density (J_0) can be calculated using the following formula:

$$J_0 = \frac{RT}{nFR_{CT}} \tag{6}$$

Here, R is the gas constant, T is temperature, n is number of electrons involved in the reaction, and R_{CT} is the charge transfer resistance.[46,47] It is evident from the figure that the CuS CEs show larger slope than Pt CE, which suggests that there is a high exchange current density (J_0) for CuS CEs as compared to that of Pt. The higher electrocatalytic activity of CuS CEs in the reduction of polysulfide electrolyte is evident from its high J_{lim} as compared to that of Pt CE. Among the CuS CEs, CE4 has very high slope and $J_{lim.}$ CE4 has a steeper change in slope, and it hits a maximum current density as the curve reaches a plateau which further supports its high electrocatalytic activity; on the contrary, Pt CE has its I_{corr} shifted toward the cathodic side revealing that it has more reduction than oxidation due to catalytic poisoning.

In order to investigate the electrocatalytic activity and the photovoltaic performance of the CuS CEs solar cells with TiO_2/CdS/CdSe/ZnS, cascade photoanodes were fabricated, and I−V measurements were carried out to compare with Pt. Figure 3d shows the UV absorption spectra of TiO_2/CdS/CdSe cascade photoanode deposited by SILAR method. From the picture, it is evident that the UV absorption for CdS5 + CdSe8 cycles exhibit extended light absorption until 625 nm. Even though further increase in the number of SILAR cycles leads to longer wavelength light absorption, the photovoltaic performance is getting reduced, and hence, our optimized deposition was fixed at CdS5 + CdSe8 cycles. Figure 4 shows the current density−voltage (J−V) plots of QDSSCs based on CuS CEs

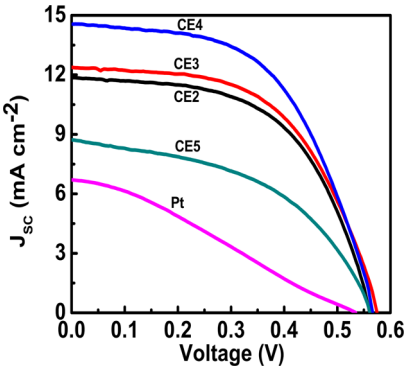

Figure 4. *I*−*V* behavior for TiO_2/CdS/CdSe/ZnS QDSSCs based on CuS and Pt counter electrodes.

and Pt under 1 sun illumination, and the corresponding photovoltaic parameters extracted from the *J*−*V* curve are shown in Table 1. From the photovoltaic performance of the QDSSCs, it is found that all the devices fabricated with CuS CEs are found to be far better than that of Pt CE due to catalytic poisoning on the Pt CE surface.[18,26,48] The enhanced electrocatalytic activity of the CuS CEs arises as a result of very weak van der Waals forces[49] between S−S layers which can readily interact with anions and cations electrochemically. The QDSSC with Pt CE shows J_{SC}, V_{OC}, and FF values of 6.671 mA cm^{-2}, 0.559 V, and 31.22%, respectively, giving a very low conversion efficiency (η) of 1.45% . On the contrary, the photovoltaic performance of QDSSC with CE4 is superior to all other CEs with J_{SC}, V_{OC}, and FF values of 14.584 mA cm^{-2}, 0.566 V, and 54.57% and has the highest η of 4.53%. This proves that CuS is the best alternative to Pt as counter electrode. The photovoltaic performance of QDSSCs with other CuS CE2, CE3, and CE5 outperformed Pt CE as their η values were found to be 3.74%, 3.94%, and 2.35%, respectively. The improvement in the J_{SC}, V_{OC}, and η is due to increased charge transfer at the CuS CE/electrolyte interface and reduced recombination, internal resistance, and electrolyte's concentration gradient.[32,37] All the QDSSCs invariably show increase in J_{SC} with increase in η. In a comparison of the photovoltaic performance of CuS CE, increase in electrocatalytic activity occurs until the deposition time is 4 h and drastically reduces after 4 h. This is due to the change in the surface morphology of CuS thin films where CE2 and CE3 show a less dense array of a CuS bunch of nanoplatelets with tubelike structure as compared to CE4 with well-knit coir mat structure with uniform pores. Apart from surface morphology, the increase in the atomic ratio % of S in Cu:S might also play a vital role in increasing the electrocatalytic activity of the CE. The S % in CE4 is the highest at 41.27:58.73 (Cu:S), and it has the well-arranged densely packed knit coir mat structure with uniform pores giving the electrolyte the ability to diffuse more freely.

To further support the electrocatalytic ability and the enhanced redox reaction at the CE/electrolyte interface, cyclic voltammetry (CV) measurements were carried out using three-electrode system. The CuS samples synthesized through CBD and Pt were drop-casted onto the glassy carbon (working) electode with nafion membrane as the binder, standard calomel electrode (SCE) as the reference electrode, and Pt as the counter elecrtorde, while 0.1 M KCl, 0.1 M Na_2S, and 0.1 M S mixture was used as the elctrolyte. Figure 5a shows the CV of CuS CEs while the inset corresponds to that of Pt. The current density obtained for the CuS CEs is higher than Pt in by many

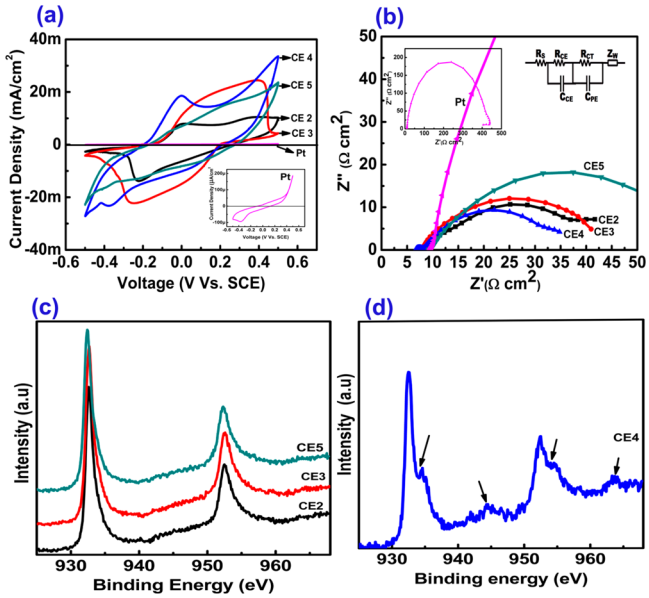

Figure 5. (a) Cyclic voltammogram of CuS at a scan rate of 20 mV s^{-1} exhibiting different redox behavior. Inset shows CV of Pt exhibiting irreversibility. (b) Nyquist plot of TiO_2/CdS/CdSe/ZnS QDSSCs for CuS and Pt counter electrodes. Inset shows the equivalent circuit and magnified plot for Pt. (c) X-ray photon spectroscopy (XPS) of Cu spectra for CuS thin films CE2, CE3, and CE5. (d) X-ray photon spectroscopy (XPS) of Cu spectrum for CuS thin film CE4.

fold. When compared with CuS CEs, Pt has very less electrocatalyic activity in polysulfide electrolyte caused by its irreversibility and overpotential[18] due to physisorption. CE4 shows the highest current density and good reversibility accounting for its better electrocatalytic activity, evidencing its best photovoltaic performance in QDSSC. This results from its surface morphology, surface roughness,[50] increased surface to volume ratio from surface uniformity,[51] and better carrier concentration enriched by the sulfur ions' presence as well. Both CE2 and CE3 show a considerable amount of reversibility with the shift of redox peaks and reduced current density, but CE5 exhibits a much lesser electrocatalytic activity with the redox peaks being diminished as a result of coir-mat-like structure without any pore restricting the flow of the electrolyte.

To throw more light on the QDSSCs' performance and to characterize their interfacial charge transfer kinetics of QDSSC, electrochemical impedance spectroscopy (EIS) was employed and is shown in Figure 5b. The Nyquist plots (Z^*) are obtained for the frequency range 100 mHz−500 kHz. The Z^* plot measured at open circuit voltage V_{OC} (light condition) has two semicircles with nonzero intercept at high frequency end. The impedance data spectra were fit using impedance spectra analysis software Z VIEW based on the equivalent circuit, having two RC circuits along with Warburg's impedance (Z_W). In order to account for the nonzero intercept on the real axis of the impedance plot to represent the sheet resistance of the FTO substrate, a series resistance is added to the circuit. In the circuit R_{CE} represents electron transfer resistance at the counter electrode/polysulfide electrolyte interface, R_{CT} represents charge transfer resistance at the photoanode/polysulfide electrolyte interface, C_{PE} is the chemical capacitance related to large number of photoexcited charge carriers in the conduction band of the photoanode resulting from very low

recombination, and Z_W is the diffusion resistance. The electron lifetime τ_S is also calculated from the midfrequency value (f_{max}) using the following formula:

$$\tau_S = \frac{1}{2\pi f_{max}} \quad (7)$$

The EIS parameters inferred from the fit and electron lifetime (τ_S) calculated are shown in Table 1. This shows that CE4 based QDSSC fabricated has much lower R_{CT} (1.843 Ω) and Z_w (0.546 Ω) proving its better electrocatalytic activity and resulting in enhanced electron transfer from the CE to the polysulfide electrolyte. In addition to that, CE4 has very low Z_W (0.546 Ω) indicating more electrolyte diffusion, resulting in increased FF (54.57%), and the high C_{PE} (62.24 μF) results from promotion of large number of photoexcited charge carrier to the conduction band of the photoanode arising from low recombination rate. Moreover, its τ_S (41.94 ms) which is inversely proportional to the f_{max} supports its faster diffusion rate and lifetime prohibiting electron recombination which make it perform better resulting in an efficiency of 4.53%. In comparison, Pt CE based QDSSC exhibits a very high R_{CE} (12.32 Ω), Z_W (10.2 Ω) results in very poor efficiency, and the high Z_w is due to the catalytic poisoning of the CE with polysulfide making it unstable and reducing the FF.[47,48] The CuS based QDSSCs has a high J_{Sc} and FF due to very low charge transfer resistance of the CuS. CE2 and CE3 show almost similar response while CE5 shows very low current density and FF due to (1) negative corrosion potential (−0.024 V), (2) lower exchange current density, and (3) anodic (β_a) slope being higher than cathodic (β_C) slope in the Tafel plot shown in Figure 3c. Negative corrosion potential implies that the quasi-Fermi-energy in CE5 would have been shifted upward and −0.024 V is essential to equilibrate the quasi-Fermi-energy with redox potential of the electrolyte.[31] The higher anodic slope tells us that oxidation predominates reduction, and hence, QD regenation rate in QDSSC would be severely affected leading to very low current density.[23,26,29] Again, the very low exchange current density (Tafel) in CE5 among CuS shows that CE5 is a poor electrocatalytic CE. Except CE4, all the other CuS CEs have their negative corrosion potential. This shift toward the cathodic side alters the band structure and flat band potential[51] and in turn the redox potential which can be seen from the presence of only reduction peak in the CV. Therefore, they need to attain equilibrium prior to their electrocatalytic activity. On the other hand, CE4 is already in equilibrium and readily reduces the polysulfide electrolyte as compared to the other CEs. Even though all cell photoanodes were similar, resistances at the interface are different because the cell operation is in a cyclic nature from QD excitation due to charge transfer to anodes and reduction of polysulfide electrolyte, and the circuit is being completed by regeneration of QDs due to oxidation of the electrolyte.[49] If the reduction and/or oxidation rate of the electrolyte is affected due to poor electrocatalytic activity of the CE, all the other sequencial behaviors of the cells would be affected. If we presume that surface area is the only cause for the reduction rate of electrolyte, then CE2 and CE3 should have produced high electrocatalytic activity; however, this is not the case here. Hence, in addition to surface area, the increase in the atomic ratio of S in CuS plays a vital role in increasing the electrocatalytic activity of the CE. As S at. % increases, Cu vacancy increases with increase in conductivity.[40]

Figure 5c shows the XPS spectra of Cu in the binding energy range 925−975 eV for CE2, CE3, and CE5 and Figure 5d for CE4. All the films show the BE peaks at 932.5 and 952.3 eV corresponding to Cu $2p_{3/2}$ and $2p_{1/2}$, respectively. However, CE4 only shows peaks at 934 eV, and the satellite peaks (marked in arrow) in between Cu $2p_{3/2}$ and $2p_{1/2}$ correspond to mixed Cu^{2+} and Cu^{+} vacancies.[40,52] Hence, Cu vacancies exist only for the films deposited at 4 h (CE4) suggesting that the conductivity would have been increased which in turn reduced the R_{CE} for CE4 at the CE/electrolyte interface.

The stability of the best performing cell is carried out by exposing it to light illumination for 20 h continuously. From Figure 6, it is vivid that the decrease in the efficiency was found

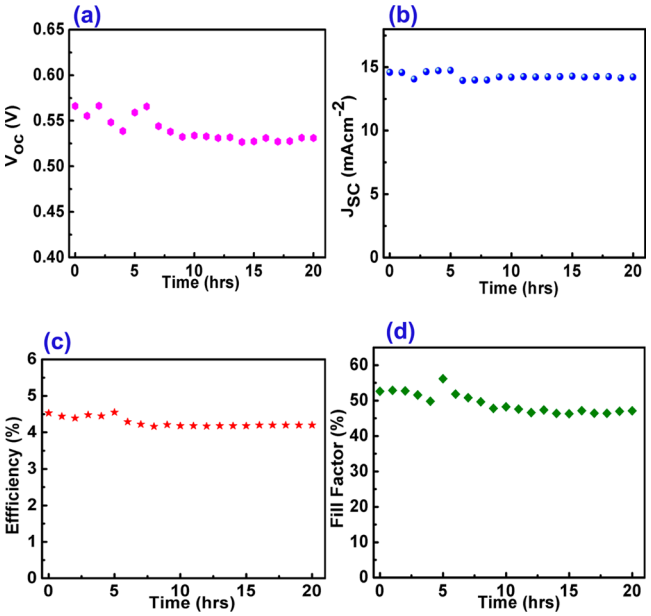

Figure 6. Comparison of $I-V$ parameters variation with aging time for the QDSSC assembled with CE4: (a) open circuit voltage, (b) short current density, (c) efficiency, (d) fill factor.

to be only 3.3% while the other parameters such as V_{OC}, FF, and J_{SC} also did not show much decrease. The better photovoltaic performance of the CE4 is attributed to the enhanced electrocatalytic activity due to (i) surface morphology of well-aligned packed knit coir mat structure with uniform pores, (ii) the increase in S at. % which increased Cu vacancy with increased conductivity enabling better reduction of polysulfide electrolyte because of its readiness to react electrochemically due to the weak van der Waals forces between S−S layers,[53] and (iii) the mixed vacancy of copper (Cu^{+} and Cu^{2+}).

5. CONCLUSION

In summary, a one-step synthetic route to a densely packed array of knit coir mat structured CuS CEs via simple chemical bath deposition is developed. As the deposition time is increased, the ratio of Cu:S and surface morphology is affected. The conductivity is increased with increase in Cu vacancy, which is turn produced very low R_s, R_{CE}, and R_{CT} for CE4. It shows a mixed oxidation state of Cu^{+} and Cu^{2+}. The weak van der Waals forces between S−S layers keeps them highly reactive with any charged species. This gives it better electrocatalytic and photocatalytic activity toward the reduction of polysulfide

electrolyte than Pt, with adequate durability. Therefore, CuS is a promising cost-effective counter electrode material for QDSSCs.

AUTHOR INFORMATION

Corresponding Author

*E-mail: prabakar@pusan.ac.kr.

Notes

The authors declare no competing financial interest.

ACKNOWLEDGMENTS

One of the authors (A.D.S.) would like to thank the National Institute for International Education (NIIED) for the fellowship. This work was supported by Basic Science Research Program through the National Research Foundation of Korea (NRF) grant funded by the Korea government (No. 2014005051).

REFERENCES

(1) O'Regan, B.; Gratzel, M. A Low-Cost, High-Efficiency Solar Cell Based on Dye-Sensitized Colloidal TiO_2 Films. *Nature* **1991**, *353*, 737−740.

(2) Kamat, P. V. Meeting the Clean Energy Demand: Nanostructure Architectures for Solar Energy Conversion. *J. Phys. Chem. C* **2007**, *111*, 2834−2860.

(3) Kamat, P. V. Quantum Dot Solar Cells. Semiconductor Nanocrystals as Light Harvesters. *J. Phys. Chem. C* **2008**, *112*, 18737−18753.

(4) Chang, J.; Su, L.; Li, C.; Chang, C.; Lin, J. Efficient "Green" Quantum Dot-Sensitized Solar Cells Based on Cu_2S-$CuInS_2$-ZnSe Architecture. *Chem. Commun.* **2012**, *48*, 4848−4850.

(5) Kongkanand, A.; Tvrdy, K.; Takechi, K.; Kuno, M.; Kamat, P. V. Quantum Dot Solar Cells. Tuning Photoresponse Through Size and Shape Control of CdSe-TiO_2 Architecture. *J. Am. Chem. Soc.* **2008**, *130*, 4007−4015.

(6) Schaller, R. D.; Klimov, V. I. High Efficiency Carrier Multiplication in PbSe Nanocrystals: Implications for Solar Energy Conversion. *Phys. Rev. Lett.* **2004**, *92*, 186601.

(7) Schaller, R. D.; Agranovich, V. M.; Klimov, V. I. High-Efficiency Carrier Multiplication Through Direct Photogeneration of Multi-Excitons via Virtual Single-Exciton States. *Nat. Phys.* **2005**, *1*, 189−194.

(8) Ross, R. T.; Nozik, A. J. Efficiency of Hot-Carrier Solar Energy Converters. *J. Appl. Phys.* **1982**, *53*, 3813−3818.

(9) Li, L.; Yang, X.; Gao, J.; Tian, H.; Zhao, J.; Hagfeldt, A.; Sun, L. Highly Efficient CdS Quantum Dot-Sensitized Solar Cells Based on a Modified Polysulfide Electrolyte. *J. Am. Chem. Soc.* **2011**, *133*, 8458−8460.

(10) Raj, C. J.; Prabakar, K.; Karthick, S. N.; Hemalatha, K. V.; Son, M.; Kim, H. Banyan Root Structured Mg-Doped ZnO Photoanode Dye-Sensitized Solar Cells. *J. Phys. Chem. C* **2013**, *117*, 2600−2607.

(11) Zhu, P.; Reddy, M. V.; Wu, Y.; Peng, S.; Yang, S.; Nair, A. S.; Loh, K. P.; Chowdari, B. V. R.; Ramakrishna, S. Mesoporous SnO_2 Agglomerates with Hierarchical Structures as an Efficient Dual-Functional Material for Dye-Sensitized Solar Cells. *Chem. Commun.* **2012**, *48*, 10865−10867.

(12) Le Viet, A.; Jose, R.; Reddy, M. V.; Chowdari, B. V. R.; Ramakrishna, S. Nb_2O_5 Photoelectrodes for Dye-Sensitized Solar Cells: Choice of the Polymorph. *J. Phys. Chem. C* **2010**, *114*, 21795−21800.

(13) Samadpour, M.; Irajizad, A.; Taghavinia, N.; Molaei, M. A. New Structure to Increase the Photostability of CdTe Quantum Dot Sensitized Solar Cells. *J. Phys. D: Appl. Phys.* **2011**, *44*, 045103.

(14) Jovanovski, V.; Gonzalez-Pedro, V.; Gimenez, S.; Azaceta, E.; Cabanero, G.; Grande, H.; Tena-Zaera, R.; Mora-Sero, I.; Bisquert, J. A Sulfide/Polysulfide-Based Ionic Liquid Electrolyte for Quantum Dot-Sensitized Solar Cells. *J. Am. Chem. Soc.* **2011**, *133*, 20156−20159.

(15) Shalom, M.; Dor, S.; Ruhle, S.; Grinis, L.; Zaban, A. Core/CdS Quantum Dot/Shell Mesoporous Solar Cells with Improved Stability and Efficiency Using an Amorphous TiO_2 Coating. *J. Phys. Chem. C* **2009**, *113*, 3895−3898.

(16) Hodes, G. Comparison of Dye- and Semiconductor-Sensitized Porous Nanocrystalline Liquid Junction Solar Cells. *J. Phys. Chem. C* **2008**, *112*, 17778−17787.

(17) Wang, Y.; Wang, D.; Jiang, Y.; Chen, H.; Chen, C.; Ho, K.; Chou, H.; Chen, C. FeS_2 Nanocrystal Ink as a Catalytic Electrode for Dye-Sensitized Solar Cells. *Angew. Chem., Int. Ed.* **2013**, *52*, 6694−6698.

(18) Radich, J. G.; Dwyer, R.; Kamat, P. V. Cu_2S Reduced Graphene Oxide Composite for High-Efficiency Quantum Dot Solar Cells. Overcoming the Redox Limitations of S_2^{-}/S_n^{2-} at the Counter Electrode. *J. Phys. Chem. Lett.* **2011**, *2*, 2453−2460.

(19) Hodes, G.; Manassen, J.; Cahen, D. Photo-Electrochemical Energy Conversion: Electrocatalytic Sulphur Electrodes. *J. Appl. Electrochem.* **1977**, *7*, 181−182.

(20) Hodes, G.; Manassen, J.; Cahen, D. Electrocatalytic Electrodes for the Polysulfide Redox System. *J. Electrochem. Soc.* **1980**, *127*, 544−549.

(21) Loucka, T. Adsorption and Oxidation of Organic Compounds on a Platinum- Electrode Partly Covered by Adsorbed Sulphur. *J. Electroanal. Chem.* **1972**, *36*, 355−367.

(22) Guo, W.; Chen, C.; Ye, M.; Lv, M.; Lin, C. Carbon Fiber/Co_9S_8 Nanotube Arrays Hybrid Structures for Flexible Quantum Dot-Sensitized Solar Cells. *Nanoscale* **2014**, *6*, 3656−3663.

(23) Gonzalez-Pedro, V.; Xu, X.; Mora-Sero, I.; Bisquert, J. Modeling High-Efficiency Quantum Dot Sensitized Solar Cells. *ACS Nano* **2010**, *4*, 5783−5790.

(24) Yu, X.; Lei, B.; Kuang, D.; Su, C. High Performance and Reduced Charge Recombination of CdSe/CdS Quantum Dot-Sensitized Solar Cells. *J. Mater. Chem.* **2012**, *22*, 12058−12063.

(25) Chen, H.; Zhu, L.; Liu, H.; Li, W. ITO Porous Film-Supported Metal Sulfide Counter Electrodes for High-Performance Quantum-Dot-Sensitized Solar Cells. *J. Phys. Chem. C* **2013**, *117*, 3739−3746.

(26) Yang, Z.; Chen, C.; Liu, C.; Li, C.; Chang, H. Quantum Dot-Sensitized Solar Cells Featuring CuS/CoS Electrodes Provide 4.1% Efficiency. *Adv. Energy Mater.* **2011**, *1*, 259−264.

(27) Tachan, Z.; Shalom, M.; Hod, I.; Ruhle, S.; Tirosh, S.; Zaban, A. PbS as a Highly Catalytic Counter Electrode for Polysulfide-Based Quantum Dot Solar Cells. *J. Phys. Chem. C* **2011**, *115*, 6162−6166.

(28) Lee, H. J.; Chen, P.; Moon, S.; Sauvage, F.; Sivula, K.; Bessho, T.; Gamelin, D. R.; Comte, P.; Zakeeruddin, S. M.; Seok, S. I.; Gratzel, M.; Nazeeruddin, M. K. Regenerative PbS and CdS Quantum Dot Sensitized Solar Cells with a Cobalt Complex as Hole Mediator. *Langmuir* **2009**, *25*, 7602−7608.

(29) Hao, F.; Dong, P.; Zhang, J.; Zhang, Y.; Loya, P. E.; Hauge, R. H.; Li, J.; Lou, J.; Lin, H. High Electrocatalytic Activity of Vertically Aligned Single-Walled Carbon Nanotubes Towards Sulfide Redox Shuttles. *Sci. Rep.* **2012**, *2*, 368.

(30) Wang, H.; Hu, Y. H. Graphene as a Counter Electrode Material for Dye-Sensitized Solar Cells. *Energy Environ. Sci.* **2012**, *5*, 8182−8188.

(31) Sudhagar, P.; Ramasamy, E.; Cho, W.; Lee, J.; Kang, Y. S. Robust Mesocellular Carbon Foam Counter Electrode for Quantum-Dot Sensitized Solar Cells. *Electron. Commun.* **2011**, *13*, 34−37.

(32) Lin, C.; Teng, C.; Li, T.; Lee, Y.; Teng, H. Photoactive p-Type PbS as a Counter Electrode for Quantum Dot-Sensitized Solar Cells. *J. Mater. Chem. A* **2013**, *1*, 1155−1162.

(33) Yang, Z.; Chen, C.; Liu, C.; Chang, H. Electrocatalytic Sulfur Electrodes for CdS/CdSe Quantum Dot-Sensitized Solar Cells. *Chem. Commun.* **2010**, *46*, 5485−5487.

(34) Deng, M.; Huang, S.; Zhang, Q.; Li, D.; Luo, Y.; Shen, Q.; Toyoda, T.; Meng, Q. Screen-Printed Cu_2S-Based Counter Electrode for Quantum-Dot-Sensitized Solar Cell. *Chem. Lett.* **2010**, *39*, 1168−1170.

(35) Huang, X.; Huang, S.; Zhang, Q.; Guo, X.; Li, D.; Luo, Y.; Shen, Q.; Toyoda, T.; Meng, Q. A Flexible Photoelectrode for CdS/CdSe

Quantum Dot-Sensitized Solar Cells (QDSSCs). *Chem. Commun.* **2011**, *47*, 2664−2666.
(36) Mane, R. S.; Lokhande, C. D. Chemical Deposition Method for Metal Chalcogenide Thin Films. *Mater. Chem. Phys.* **2000**, *65*, 1−31.
(37) Kalanur, S. S.; Chae, S. Y.; Joo, O. S. Transparent $Cu_{1.8}S$ and CuS Thin Films on FTO as Efficient Counter Electrode for Quantum Dot Solar Cells. *Electrochim. Acta* **2013**, *103*, 91−95.
(38) Lukashev, P.; Lambrecht, W. R. L.; Kotani, T.; van Schilfgaarde, M. Electronic and Crystal Structure of $Cu_{2-x}S$: Full-Potential Electronic Structure Calculations. *Phys. Rev. B* **2007**, *76*, 195202.
(39) Luther, J. M.; Jain, P. K.; Ewers, T.; Alivisatos, A. P. Localized Surface Plasmon Resonances Arising from Free Carriers in Doped Quantum Dots. *Nat. Mater.* **2011**, *10*, 361−366.
(40) Kundu, M.; Hasegawa, T.; Terabe, K.; Aono, M. Effect of Sulfurization Conditions on Structural and Electrical Properties of Copper Sulfide Films. *J. Appl. Phys.* **2008**, *103*, 073523−1−073523−7.
(41) Li, G.; Liu, M.; Liu, H. Controlled Synthesis of Porous Flowerlike Cu_2S Microspheres with Nanosheet-Assembly. *Cryst. Eng. Commun.* **2011**, *13*, 5337−5341.
(42) Abdelhady, A. L.; Ramasamy, K.; Malik, M. A.; O'Brien, P.; Haigh, S. J.; Raftery, J. New Routes to Copper Sulfide Nanostructures and Thin Films. *J. Mater. Chem.* **2011**, *21*, 17888−17895.
(43) Zhao, Y.; Pan, H.; Lou, Y.; Qiu, X.; Zhu, J.; Burda, C. Plasmonic $Cu_{2-x}S$ Nanocrystals: Optical and Structural Properties of Copper-Deficient Copper(I) Sulfides. *J. Am. Chem. Soc.* **2009**, *131*, 4253−4261.
(44) Justin Raj, C.; Prabakar, K.; Dennyson Savariraj, A.; Kim, H. Surface Reinforced Platinum Counter Electrode for Quantum Dots Sensitized Solar Cells. *Electrochim. Acta* **2013**, *103*, 231−236.
(45) Eda, S.; Moriyasu, K.; Fujishima, M.; Nomura, S.; Tada, H. Photodeposition of Copper Sulphide Nanocrystals on Titanium(IV) Oxide Nanorods and Their Application in Smart Windows. *RSC Adv.* **2013**, *3*, 10414−10419.
(46) Hauch, A.; Georg, A. Diffusion in the Electrolyte and Charge-Transfer Reaction at the Platinum Electrode in Dye-Sensitized Solar Cells. *Electrochim. Acta* **2001**, *46*, 3457−3466.
(47) Banerjee, A.; Upadhyay, K. K.; Bhatnagar, S.; Tathavadekar, M.; Bansode, U.; Agarkar, S.; Ogale, S. B. Nickel Cobalt Sulfide Nanoneedle Array as an Effective Alternative to Pt as a Counter Electrode in Dye Sensitized Solar Cells. *RSC Adv.* **2014**, *4*, 8289−8294.
(48) Chakrapani, V.; Baker, D.; Kamat, P. V. Understanding the Role of the Sulfide Redox Couple (S^{2-}/S_n^{2-}) in Quantum Dot-Sensitized Solar Cells. *J. Am. Chem. Soc.* **2011**, *133*, 9607−9615.
(49) Kamat, P. V. Quantum Dot Solar Cells. The Next Big Thing in Photovoltaics. *J. Phys. Chem. Lett.* **2013**, *4*, 908−918.
(50) Wu, M.; Lin, X.; Hagfeldt, A.; Ma, T. A Novel Catalyst of WO_2 Nanorod for the Counter Electrode of Dye-Sensitized Solar Cells. *Chem. Commun.* **2011**, *47*, 4535−4537.
(51) Feng, X.; Shankar, K.; Paulose, M.; Grimes, C. A. Tantalum-Doped Titanium Dioxide Nanowire Arrays for Dye-Sensitized Solar Cells with High Open-Circuit Voltage. *Angew. Chem., Int. Ed.* **2009**, *48*, 8095−8098.
(52) Zaman, M. S.; Grajeda, G. B.; Haberer, E. D. Optical and Electrical Stability of Viral-Templated Copper Sulfide ($Cu_{1.8}S$) films. *J. Appl. Phys.* **2014**, *115*, 144311.
(53) Rui, X.; Tan, H.; Yan, Q. Nanostructured Metal Sulfides for Energy Storage. *Nanoscale* **2014**, *6*, 9889−9924.